Title

Chapter Three 3D Structures of Fungal Partitiviruses

Authors

Nibert, Max L
Tang, Jinghua
Xie, Jiatao
et al.

Publication Date

2013

DOI

10.1016/b978-0-12-394315-6.00003-9

Peer reviewed

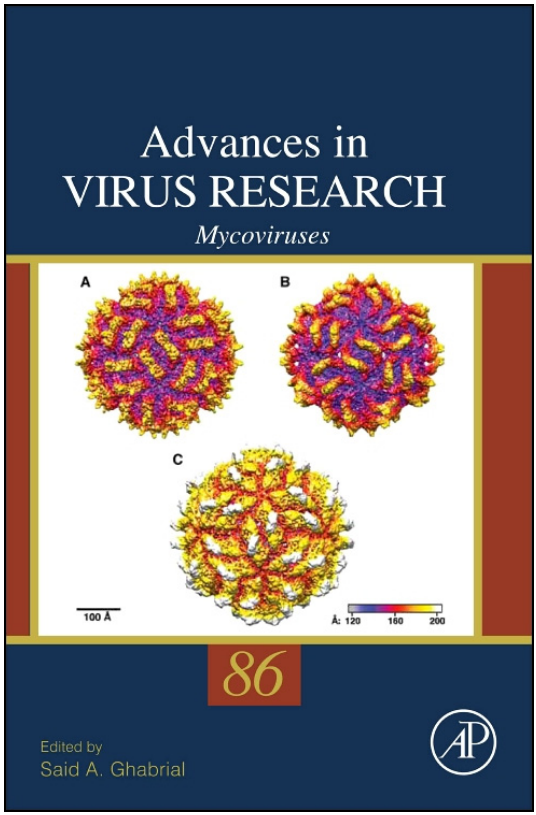

From: Max L. Nibert, Jinghua Tang, Jiatao Xie, Aaron M. Collier, Said A. Ghabrial, Timothy S. Baker and Yizhi J. Tao, 3D Structures of Fungal Partitiviruses.
In Said A. Ghabrial, editor: *Advances in Virus Research,* Vol. 86, Burlington: Academic Press, 2013, pp. 59-85.
ISBN: 978-0-12-394315-6

CHAPTER THREE

3D Structures of Fungal Partitiviruses

Max L. Nibert[*,1,2], Jinghua Tang[†], Jiatao Xie[‡], Aaron M. Collier[§], Said A. Ghabrial[‡,2], Timothy S. Baker[†,2] and Yizhi J. Tao[§,2]

[*]Department of Microbiology and Immunobiology, Harvard Medical School, Boston, Massachusetts, USA
[†]Department of Chemistry and Biochemistry, and Division of Biological Sciences, University of California–San Diego, La Jolla, California, USA
[‡]Department of Plant Pathology, University of Kentucky, Lexington, Kentucky, USA
[§]Department of Biochemistry and Cell Biology, Rice University, Houston, Texas, USA
[1]Corresponding author: e-mail address: mnibert@hms.harvard.edu
[2]Co-senior authors

Contents

Abstract

Partitiviruses constitute one of the nine currently recognized families of viruses with encapsidated, double-stranded (ds)RNA genomes. The partitivirus genome is bisegmented, and each genome segment is packaged inside a separate viral capsid. Different partitiviruses infect plants, fungi, or protozoa. Recent studies have shed light on the three-dimensional structures of the virions of three representative fungal partitiviruses. These structures include a number of distinctive features, allowing informative comparisons with the structures of dsRNA viruses from other families. The results and comparisons suggest several new conclusions about the functions, assembly, and evolution of these viruses.

Since May 2008, we have reported the three-dimensional (3D) structures of three fungal viruses from the dsRNA virus family *Partitiviridae*: Penicillium stoloniferum virus S (PsV-S), Penicillium stoloniferum virus F (PsV-F), and

Advances in Virus Research, Volume 86
ISSN 0065-3527
http://dx.doi.org/10.1016/B978-0-12-394315-6.00003-9

Fusarium poae virus 1 (FpV1) (Ochoa et al., 2008; Pan et al., 2009; Tang, Ochoa, et al., 2010; Tang, Pan, et al., 2010). This work has represented the collaborative efforts of four laboratories, whose principal investigators are noted as co-senior authors of this review. The work was first begun in late 2006 upon recognition of the fact that no 3D structures of partitiviruses had been reported at that time, and indeed ours remain the only such structures reported through the present. As discussed below, the three fungal partitiviruses we have analyzed most likely represent two different taxonomic genera, leaving partitiviruses from several other genera yet to be analyzed for structural comparisons across the whole family. Among those partitiviruses from other genera are ones that infect distinct hosts, namely, plants and the apicomplexan protozoan *Cryptosporidium*. Thus, a good deal of structural diversity within this family may remain to be discovered. In this review, after briefly introducing the partitiviruses, we summarize the major structural features of the three analyzed strains, compare these 3D structures to those of other encapsidated dsRNA viruses, and discuss the implications of these structures for viral functions, assembly, and evolution.

1. INTRODUCTION TO PARTITIVIRUSES

Fungal, plant, and protozoan partitiviruses have bisegmented genomes, comprising two distinct, linear dsRNA molecules, each 1.4–2.3 kbp in length for a total genome length of 3.1–4.4 kbp (reviewed by Ghabrial, Ochoa, Baker, & Nibert, 2008, Ghabrial et al., 2011). The two genome segments encode two proteins: one, the viral coat protein (CP) and, the other, the viral RNA-dependent RNA polymerase (RdRp). Notably, each of these segments is packaged inside a separate, though presumably identical, viral capsid, meaning that not only is the genome bisegmented but also the infectious unit is at minimum biparticulate. Partitiviruses are thought to undergo efficient, natural transmission between host cells only through intracellular means, such as during cell division (mitosis, meiosis) or cell–cell fusion (hyphal anastomosis), which allow transfer of multiple virus particles to each new cell. Natural transmission by cell-penetrating insect or other vectors that feed on virus-infected host cells, as known for many plant viruses, is also conceivable but has yet to be demonstrated for partitiviruses. Encapsidated satellite dsRNAs, which are dependent on helper virus for replication, are associated with some partitiviruses, including PsV-F and FpV1 (Compel, Papp, Bibo, Fekete, & Hornok, 1999; Kim, Choi, & Lee, 2005).

Taxonomically, the family *Partitiviridae* currently comprises four genera: *Partitivirus*, *Alphacryptovirus*, *Betacryptovirus*, and *Cryspovirus* (Ghabrial et al., 2008, 2011; Nibert, Woods, Upton, & Ghabrial, 2009; Fig. 3.1). Recognized members of the genus *Partitivirus* infect fungi, those of the genera *Alphacryptovirus* and *Betacryptovirus* infect plants, and those of the genus *Cryspovirus* infect protozoa (*Cryptosporidium* species). As discussed below, however, this current taxonomic and classification scheme has become subject to several criticisms as the number of partitivirus isolates and genome sequences have grown in recent years. Thus, some reworking of the genera and their characteristic features within this family appears warranted.

Penicillium stoloniferum viruses PsV-S and PsV-F are both members of the genus *Partitivirus* and can coinfect the saprophytic ascomycete *Penicillium stoloniferum*. Each encodes an ~47-kDa CP and an ~62-kDa RdRp, but the amino acid (aa) sequences of these proteins are readily distinguishable, exhibiting only 19% and 27% identity, respectively (Kim et al., 2005, Kim, Kim, & Kim, 2003; Tang, Ochoa, et al., 2010). They are also distinguishable by serological reactivities (Bozarth, Wood, & Mandelbrot, 1971). The respective names PsV-S and PsV-F reflect the relative electrophoretic mobilities of their particles on agarose gels: S, slow; F, fast (Bozarth et al., 1971). The genome of PsV-S comprises a 1754-bp dsRNA1, encoding the 539-aa RdRp, and a 1582-bp dsRNA2, encoding the 434-aa CP (Kim et al., 2003), whereas the genome of PsV-F comprises a 1677-bp dsRNA1, encoding the 538-aa RdRp, and a 1500-bp dsRNA2, encoding the 420-aa CP (Kim et al., 2005). PsV-F, but not PsV-S, contains at least one satellite segment, the 677-bp dsRNA3, which is unrelated in sequence to the other two segments (Kim et al., 2005; Tang, Pan, et al., 2010). Although both viruses can coinfect *P. stoloniferum*, the CP of each associates only with itself in forming the respective capsids (Buck & Kempson-Jones, 1974) and packages only its own RNAs (Bozarth et al., 1971). Purified virions of both viruses exhibit semiconservative transcription activity (Buck, 1978; Pan et al., 2009), reflecting that the viral RdRp is packaged into virions along with the CP and genome segments, as is characteristic of other encapsidated dsRNA viruses.

Fusarium poae virus 1 is also a member of the genus *Partitivirus* and can infect the phytopathogenic ascomycete *Fusarium poae*, one cause of Fusarium head blight in cereal grains worldwide. This virus was originally named FUPO-1 (Compel et al., 1999) but was later renamed FpV1 for consistency with existing names for other partitiviruses (Ghabrial et al., 2008, 2011). The genome of FpV1 comprises a 2203-bp dsRNA1, encoding the

Encapsidated dsRNA viruses

Genome segments	*Family* / *Subfamily* / *Genus*	Capsids
1	***Totiviridae***	
	Giardiavirus	
	Leishmaniavirus	
	Totivirus	*T*=1(120)
	Trichomonasvirus	
	Victorivirus	
2	*Birnaviridae*	
	Avibirnavirus	
	Aquabirnavirus	*T*=13
	Blosnabirnavirus	
	Entomobirnavirus	
	Megabirnaviridae	Not reported
	Megabirnavirus	
	Partitiviridae	
	Alphacryptovirus	
	Betacryptovirus	*T*=1(120) **PsV-S PsV-F FpV1**
	Cryspovirus	
	Partitivirus	
	Picobirnaviridae	*T*=1(120)
	Picobirnavirus	
3	*Cystoviridae*	*T*=1(120) + *T*=13
	Cystovirus	
4	***Chrysoviridae***	*T*=1(60)
	Chrysovirus	
	Quadriviridae	Not reported
	Quadrivirus	
9–12	***Reoviridae***	
	Sedoreovirinae	
	Cardoreovirus	
	Mimoreovirus	
	Orbivirus	
	Phytoreovirus	
	Rotavirus	
	Seadornavirus	
	Spinareovirinae	*T*=1(120) + *T*=13
	Aquareovirus	
	Coltivirus	
	Cypovirus	
	Dinovernavirus	
	Fijivirus	
	Idnoreovirus	
	Mycoreovirus	
	Orthoreovirus	
	Oryzavirus	

Figure 3.1 Taxonomy and properties of encapsidated dsRNA viruses. Taxa that include fungal viruses are bolded. Icosahedral symmetries of the viral capsids are indicated; for $T=1$ capsids, the number in parentheses indicates whether there are 60 or 120 subunits in each capsid. Cystoviruses and reoviruses have two concentric icosahedral capsids with different symmetries as indicated; the $T=1$ capsid of each of these viruses is the one that encloses the genome (inner capsid). Viruses in certain reovirus genera may lack parts of the $T=13$ outer capsid. The $T=1(120)$ capsid structure of partitiviruses is boxed to emphasize the focus of this review, and the particular partitiviruses for which structures are described (PsV-S, etc.) are indicated beside the box.

673-aa (78-kDa) RdRp, and a 2185-bp dsRNA2, encoding the 637-aa (70-kDa) CP (Compel et al., 1998). Thus, the genome of FpV1 is ~30% longer than that of PsV-S and PsV-F, and the CP of FpV1 is ~50% larger (by molecular mass) than that of PsV-S and PsV-F. In these regards, FpV1 is similar to the prototype species of genus *Partitivirus*, *Atkinsonella hypoxylon virus* (Oh & Hillman, 1995; strain abbreviation AhV). Indeed, sequence-based phylogenetic comparisons have revealed that FpV1 and AhV belong to the same subclade of partitivirus isolates, whereas PsV-S and PsV-F are distantly related within a distinct subclade (Boccardo & Candresse, 2005; Crawford et al., 2006; Ghabrial et al., 2008, 2011; Tang, Ochoa, et al., 2010; Willenborg, Menzel, Vetten, & Maiss, 2009). These findings represent some of the compelling evidence that a taxonomic reworking of the family *Partitiviridae* is warranted, including to divide the current genus *Partitivirus* into at least two new genera. These findings, along with the fact that the level of sequence identity among the CPs of PsV-S, PsV-F, and FpV1 is quite low (identity scores between FpV1 and PsV-S or PsV-F are, respectively, 14% or 13%, versus 19% between PsV-S and PsV-F), additionally led us to predict that a 3D structure determination for FpV1 virions may reveal unique variations on the capsid architectures first revealed from our studies of PsV-S and PsV-F. FpV1 also appears to contain at least one, ~550-bp satellite segment (Compel et al., 1998; Tang, Ochoa, et al., 2010), for which a sequence has not yet been reported.

Although much remains unknown about various other aspects of partitivirus infection, a few of these are addressed in the structure-oriented discussions below.

2. PARTITIVIRUS CAPSID STRUCTURES

Prior to our recent 3D structure determinations, partitivirus virions were known from negative-stain transmission electron microscopy to be isometric and small, on the order of 30–40 nm in diameter (Bozarth et al., 1971; Buck & Kempson-Jones, 1973; Compel et al., 1998; Crawford et al., 2006). In addition, they appeared to have a single-layer capsid (not the double- or triple-layer capsids of more complex dsRNA viruses from the families *Cystoviridae* and *Reoviridae*; Fig. 3.1) and some short surface protuberances rising above the contiguous shell region. The genomic dsRNA appeared to be centrally enclosed by this shell, as inferred from the presence of less dense "empty" particles, from which the central dsRNA had seemingly been lost (or had never been present) and which were

therefore more completely penetrated by negative stain. Stoichiometric estimates based on sedimentation- and gel-based molecular weights of whole particles and CP subunits suggested the presence of ~120 CP molecules and ~1 RdRp molecule per particle in the case of fungal partitivirus PsV-S (Buck & Kempson-Jones, 1973, 1974). Based on these earlier observations and in light of more recent structure determinations for other dsRNA viruses with genome-enclosing capsids comprising 120 icosahedrally arranged subunits of their respective CPs or inner-capsid proteins (ICPs; Cheng et al., 1994; Dunn et al., 2013; Grimes et al., 1998; Huiskonen et al., 2006; McClain, Settembre, Temple, Bellamy, & Harrison, 2010; Naitow, Tang, Canady, Wickner, & Johnson, 2002; Reinisch, Nibert, & Harrison, 2000; Tang et al., 2008; Yu, Jin, & Zhou, 2008; Zhou et al., 2001), the expectation had quite reasonably been that the partitivirus capsid is another related example of one of these 120-subunit structures with $T=1$ symmetry and an icosahedral asymmetric unit (IAU) comprising a CP dimer. This is in fact what our recent 3D structure determinations have shown, though with some new aspects of interest for describing partitivirus capsids, in particular, and 120-subunit capsids of other dsRNA viruses, in general.

For our structural analyses of partitivirus virions, we began with a coinfected culture of *P. stoloniferum*, from which we differentially isolated the virions of PsV-S and PsV-F. These purified virions were then subjected to transmission electron cryomicroscopy (cryo-TEM) and 3D image reconstruction. The analysis of PsV-S progressed most quickly, and so the cryo-TEM structure of PsV-S was the first to be reported, at a nominal resolution of 7.3 Å (Ochoa et al., 2008; Fig. 3.2). In the meantime, crystals of PsV-F virions had been grown and were found to be amenable to high-resolution data collection. As a result, the second report contained not only a cryo-TEM structure of PsV-F at a nominal resolution of 8.0 Å but also a crystal structure at 3.3 Å, the latter of which provided a nearly complete atomic model for PsV-F CP (Pan et al., 2009; Fig. 3.3). For the third report, the cryo-TEM structures of both PsV-S and PsV-F were carefully refined to nominal resolutions of 4.5–4.7 Å, making use of the fitted PsV-F crystal structure for assessing progress during the refinement process, and the final PsV-S cryo-TEM map and PsV-F crystal structure were used to generate a nearly complete atomic model for PsV-S CP (Tang, Pan, et al., 2010; Fig. 3.3). To complete our studies of partitivirus structures to date, we lastly isolated FpV1 virions from a culture of *F. poae* and determined a cryo-TEM structure at a nominal resolution of 5.0 Å (Tang, Ochoa, et al., 2010;

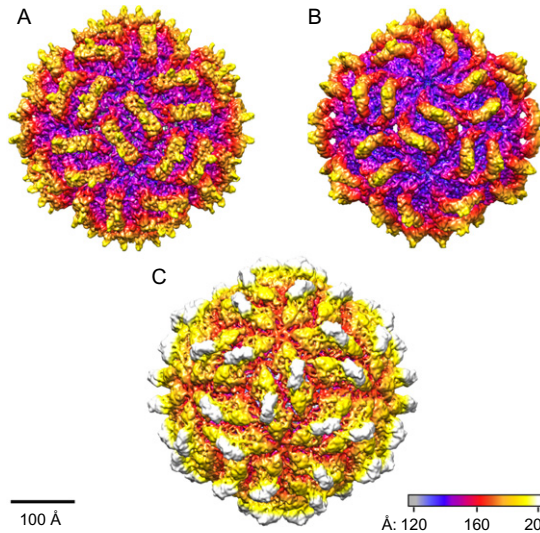

Figure 3.2 Fungal partitivirus virion structures obtained by cryo-TEM and icosahedral 3D image reconstruction. Radially color-coded surface views are shown for (A) PsV-S, (B) PsV-F, and (C) FpV1 (Pan et al., 2009; Tang, Ochoa, et al., 2010; Tang, Pan, et al., 2010). The structures are shown at the same scale (see bar at lower left), with the same radial color map (lower right; radii in Å) applied to each.

Fig. 3.2). With this set of new 3D structures in hand, we could then draw a variety of new conclusions regarding both conserved and variable elements of partitivirus structure.

The outermost diameter of each partitivirus virion ranges from 350 and 370 Å for PsV-S and PsV-F, respectively, to 420 Å for FpV1 (Fig. 3.2). The innermost diameter of the contiguous capsid shell of each virus ranges from 250 Å for both PsV-S and PsV-F to 270 Å for FpV1. Combining these two sets of data, the radial span of each capsid ranges from 100 and 120 Å for PsV-S and PsV-F, respectively, to 150 Å for FpV1. The larger diameter and span of the FpV1 capsid correlates with the ~50% larger molecular mass of its CP. In addition, the larger innermost diameter of the FpV1 capsid, and thus the larger volume of central cavity enclosed by it, correlates with the >30% greater length of each FpV1 genome segment.

The capsid of each partitivirus is formed from 120 icosahedrally arranged subunits of the respective CP. In each virus, these 120 subunits fall into two categories, reflecting two non-quasi-equivalent positions within the capsid shell (Fig. 3.3A and B). Sixty of the subunits, the so-called *A* subunits,

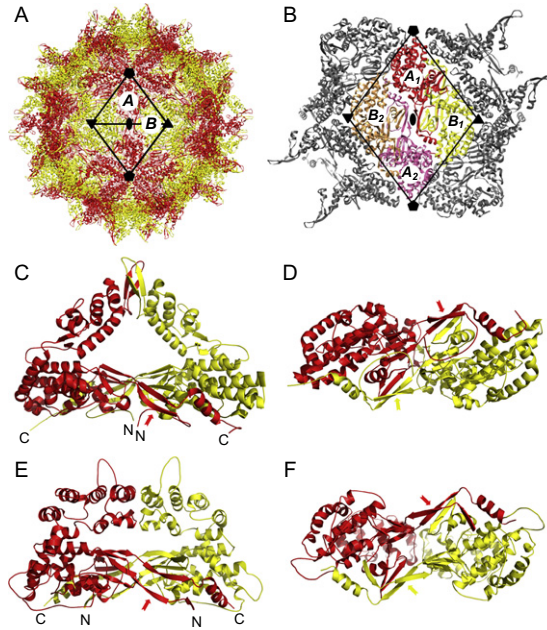

Figure 3.3 Fungal partitivirus capsid and CP structures obtained by X-ray crystallography or by cryo-TEM and homology modeling. (A) Cα trace of the PsV-F capsid structure viewed along an I2 axis. *A* and *B* subunits are colored red and yellow, respectively. I2, I3, and I5 axes are marked with symbols (oval, triangles, and pentagons) and connected by lines. (B) A CP dodecamer with two quasisymmetric *A*–*B* dimers (A_1–B_1 and A_2–B_2) differentially colored (red:yellow and magenta:orange, respectively). A_1–B_1 and A_2–B_2 extend in antiparallel fashion along either side of an I2 axis, forming a dimer of dimers (tetramer) that is largely confined within the diamond shape formed by lines connecting the I3 and I5 axes. (C–F) Views of the PsV-F quasisymmetric *A*–*B* dimer Cα trace (C and D) and the PsV-S quasisymmetric *A*–*B* dimer Cα trace (E and F) as viewed from the side (C and E) and from beneath (i.e., from inside the particle) (D and F). *A* and *B* subunits are colored red and yellow, respectively. In (C) and (E), visible N-and C-termini are labeled. Red and yellow arrows point toward β-strands involved in domain swapping, as discussed in the text. Cα traces for PsV-F and PsV-S are, respectively, from Pan et al. (2009) and Tang, Pan, et al. (2010).

approach and surround each icosahedral fivefold (I5) axis. The other 60 subunits, the so-called *B* subunits, approach and surround each icosahedral threefold (I3) axis. Both the *A* and *B* subunits approach each icosahedral twofold (I2) axis, though *A*:*A* contacts across this axis appear to predominate, as discussed further below.

One of the routine questions when describing a 120-subunit $T=1$ structure is which of the *A* and *B* subunits might be best identified as forming the

IAU, of which there are 60 such *A*–*B* dimers in the whole capsid. From previously determined structures for other dsRNA viruses (Castón et al., 1997; Grimes et al., 1998; Huiskonen et al., 2006; McClain et al., 2010; Naitow et al., 2002; Reinisch et al., 2000; Tang et al., 2008; Yu et al., 2008; Zhou et al., 2001), three good options are evident for any given *A* subunit (Fig. 3.4A). In two of these options (B_1 and B_2 in Fig. 3.4A), the *B* subunit is approximately parallel to and side-by-side with the chosen *A* subunit and is thus asymmetrically positioned relative to that *A*. In each of these two options, the resulting *A*–*B* dimer is relatively compact, and the surface area buried between the two subunits is similarly large. In the third option, the *B* subunit is antiparallel to and end-to-end with the chosen *A* subunit and is thus quasisymmetrically positioned relative to that *A* (B_3 in Fig. 3.4, left).

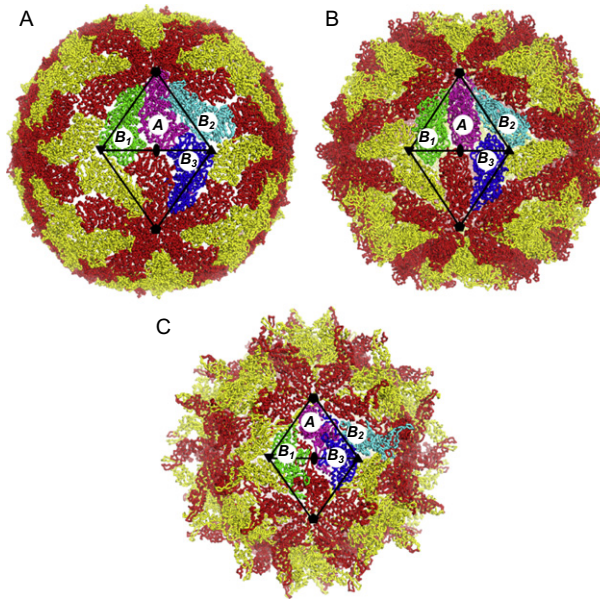

Figure 3.4 Comparison of reovirus, totivirus, and partitivirus inner capsid or capsid organizations. Shown are crystallography-derived Cα traces of (A) Bluetongue virus (family *Reoviridae*) inner capsid (Grimes et al., 1998), (B) Saccharomyces cerevisiae virus L-A (family *Totiviridae*) capsid (Naitow et al., 2002), and (C) PsV-F (family *Partitiviridae*) capsid (Pan et al., 2009). In each virus, *A* and *B* subunits are colored red and yellow, respectively. In addition, a chosen *A* subunit is labeled and colored magenta in each virus, and the three adjacent *B* subunits are colored green (B_1), cyan (B_2), and blue (B_3). The *A*–B_1 and *A*–B_2 dimers are asymmetric and the *A*–B_3 dimers are quasisymmetric in each case. *Note*: Different capsids are not shown at the same scale.

In this option, however, the resulting *A*–*B* dimer is a good deal more extended, that is, much less compact, with less buried surface area between the two subunits. In previous dsRNA virus structures, because of the compactness and greater buried surface area of each of the first two options, one of those types of asymmetric *A*–*B* dimer has been routinely chosen to represent the IAU. In partitivirus capsids, however, due in part to the smaller size of the CP shell domain, the quasisymmetric *A*–*B* dimer is not substantially less compact than the asymmetric *A*–*B* dimers, and indeed one of the asymmetric dimers is the least compact of the three options (Fig. 3.4, right). Thus, for the partitivirus capsids, choosing the quasisymmetric dimer to represent the IAU appears reasonable.

In fact, the atomic models of PsV-S and PsV-F help to address this question for partitiviruses in that there is a clear domain swapping within the shell regions of the *A* and *B* subunits in the quasisymmetric dimer of each virus (Pan et al., 2009; Tang, Pan, et al., 2010; Fig. 3.3B–F). This finding argues strongly that this particular type of *A*–*B* dimer is (i) likely to be the protomer for capsid assembly and (ii) thus well chosen to represent the IAU. Specifically, noteworthy features at this dimer interface within the capsid shell are four four-stranded β-sheets. In both PsV-S and PsV-F, two of these sheets consist of four β-strands from the same subunit, *A* or *B*, but the other two sheets are formed by two β-strands from each of the two different subunits, which thereby represents the domain swapping that suggests this dimer as the assembly promoter. Such domain swapping had not been seen in previous dsRNA virus capsid structures, but a very similar feature has also recently been found in a picobirnavirus (Duquerroy et al., 2009), as described more below.

There is in fact another striking feature in the partitivirus 3D structures that argues for the quasisymmetric *A*–*B* dimer to be the assembly promoter and thus well chosen to represent the IAU. This feature consists of a second, so-called "arch" domain in each CP subunit that represents an insertion in the middle of the shell domain of both PsV-S and PsV-S CP and protrudes on the particle surface (Pan et al., 2009; Tang, Pan, et al., 2010; Fig. 3.3C and E). An arch domain is also present in FpV1 CP, but the primary sequences that form it remain undefined in the absence of an atomic model to date (Tang, Ochoa, et al., 2010). In all three viruses, the arch domain of a given *A* subunit reaches up and over to make extensive additional contacts with, and only with, the arch domain of the *B* subunit within the quasisymmetric dimer (Fig. 3.3C and E). In both PsV-S and PsV-F, these contacts occur well above the shell surface, leaving an open solvent path

underneath, and thus the contacting arch domains in each quasisymmetric *A*–*B* dimer indeed form an arch over the underlying shell domains, for a total of 60 such arches per particle. In FpV1, the arch domains are collapsed toward the shell domain surface such that little or no solvent path is left underneath, but extensive additional contacts with, and only with, the arch domains of the *A* and *B* subunits within the quasisymmetric dimer are nonetheless made. In each virus, the arch domain contacts thus increase the molecular interface of contacts between the two subunits within this dimer, presumably adding to its stability. Whether these roles in assembly and stability are the sole functions of these arches remains to be defined, but they are such striking structural features on the particle surfaces that some additional function, such as in anchoring to some intracellular host factor, seems likely.

An additional set of observations about the PsV-S and PsV-F capsids leads to another prediction about their assembly pathways. For any given quasisymmetric *A*–*B* dimer in the capsid, the adjacent such dimer against which it buries the largest surface area (~3500 $Å^2$) is the dimer immediately across the I2 axis from it (Figs. 3.3B and 3.4B). In comparison, contacts between any two such dimers around the I3 and I5 axes bury much smaller surface areas (~2000 $Å^2$). We have therefore proposed (Pan et al., 2009; Tang, Pan, et al., 2010) that the assembly of PsV-S and PsV-F capsids likely proceeds first from quasisymmetric *A*–*B* dimers (protomers) and next to antiparallel, symmetric dimers of these dimers (Fig. 3.3B). Thirty such diamond-shaped dimers of dimers (tetramers) would then interact further via threefold and fivefold symmetry contacts to complete assembly of the 120-subunit capsid. Notably, this proposed assembly pathway for partitiviruses is quite distinct from that involving pentamers of asymmetric *A*–*B* dimers (decamers) as a key intermediate as has been previously proposed for some other dsRNA viruses (Grimes et al., 1998; McClain et al., 2010), and indeed dimers of quasisymmetric *A*–*B* dimers and pentamers of asymmetric *A*–*B* dimers represent assembly pathways that are mutually exclusive. Assembly of the cystovirus inner capsid, on the other hand, proceeds through a stable, tetramer intermediate of *A*–*B* dimers (Kainov, Butcher, Bamford, & Tuma, 2003), suggesting that cystoviruses and partitiviruses may share similar assembly pathways for their genome-enclosing capsids. Returning to describe the contacts within each symmetric dimer of dimers in partitiviruses, substantial contacts occur between the *A* subunit from one protomer and the *B* subunit from the other protomer, but the predominant contacts are between the *A* subunits from the two protomers (Fig. 3.3B). Moreover, interestingly, it is the domain-swapping

arm of each *A* subunit that mediates these predominate interactions, including those directly across each I2 axis in the assembled capsid.

It is worth noting that the partitivirus virions of each strain used for our 3D structure studies contained different dsRNA molecules: dsRNA1 or dsRNA2 and/or satellite(s). In preparing these particles for study, we did nothing extra to try to separate or enrich the particles according to specific dsRNA content. The fact that high-resolution capsid structures were nevertheless obtained, including the PsV-F crystal structure at 3.3-Å resolution, therefore indicates that the capsid of each virus does not vary to a substantial degree according to which dsRNA molecule is packaged. Instead, the overall structure of each capsid appears to be nearly identical, regardless of the respectively packaged dsRNA. Moreover, in the case of PsV-S and PsV-F, since these particles were differentially isolated from the same coinfected *P. stoloniferum* culture, the high-resolution capsid structures corroborate previous evidence that the CP of each virus associates only with itself in forming the respective capsids (Buck & Kempson-Jones, 1974), that is, that chimeric capsids are not formed to any substantial degree. Whether this specificity for self-interaction in complete capsids is maintained purely at the level of CP subunit–subunit interactions or is also aided by some sequestration of PsV-S and PsV-F CP subunits into separate compartments in coinfected cells remains an interesting question.

3. PARTITIVIRUS RdRp AND dsRNA STRUCTURES

The cryo-TEM and crystal structures described earlier tell us a great deal about the 120-subunit capsids of these fungal partitiviruses. But what about the other virion components: the RdRp and the dsRNA genome?

No structural elements attributable to the RdRp were identified in any of our partitivirus density maps, which is not surprising since there is thought to be only ~1 RdRp molecule per virion (Buck & Kempson-Jones, 1974). Furthermore, no structure of a partitivirus RdRp molecule purified in isolation has been reported to date. Thus, with regard to the RdRp, what we can say here is limited and speculative. First, conserved motifs common to the RdRps of other encapsidated dsRNA viruses (Bruenn, 1993) appear in the usual order in partitivirus RdRp sequences (Crawford et al., 2006; Ghabrial et al., 2011), suggesting that they adopt the right-hand fingers–palm–thumb configuration that is common to many RNA and DNA polymerases (Ortín & Parra, 2006). In the crystallized RdRps of other encapsidated dsRNA viruses, the catalytic hand domain spans between 440

and 590 aa (Butcher, Grimes, Makeyev, Bamford, & Stuart, 2001; Lu et al., 2008; Pan, Vakharia, & Tao, 2007; Tao, Farsetta, Nibert, & Harrison, 2002). Thus, since the overall sequence lengths of partitivirus RdRps approximate 510–680 aa, it seems likely that most of those sequences are devoted to forming the catalytic domain, with relatively limited regions of sequence available to form additional, large N- and C-terminal domains as seen in the larger RdRps of reoviruses and birnaviruses (Lu et al., 2008; Pan et al., 2007; Tao et al., 2002). The additional 64-aa C-terminal "priming" domain of cystovirus RdRp (Butcher et al., 2001), on the other hand, is probably small enough to have an equivalent in partitivirus RdRps.

Where might the RdRp be located within the partitivirus virion? Based on findings with other encapsidated dsRNA viruses (McClain et al., 2010; Sen et al., 2008; Zhang, Walker, Chipman, Nibert, & Baker, 2003), the partitivirus RdRp is likely to be located interior to the capsid, probably anchored by noncovalent interactions to the undersurface of the capsid shell. Importantly, of course, from that position it can access the RNA template for transcription. As to its specific location relative to the symmetry axes of the capsid, it is more difficult to say. In reoviruses, each copy of the RdRp is anchored nearest, and overlapping, an I5 axis of the inner capsid (McClain et al., 2010; Zhang et al., 2003). In cystovirus procapsids, however, each copy of the RdRp appears to be anchored near an I3 axis of the inner capsid, though it has been proposed that it might rotate nearer an I5 axis during particle maturation (Sen et al., 2008). In reoviruses, it furthermore appears that RNA transcripts exit through inner-capsid pores cotranscriptionally, and thus each copy of the RdRp is thought to be positioned near pentonal or peripentonal pores that allow this exit (Diprose et al., 2001; Lawton, Estes, & Prasad, 1997; Mendez, Weiner, She, Yeager, & Coombs, 2008; Yang et al., 2012; Zhang et al., 2003). From our partitivirus structures, we have seen that small ($\leq$5-Å diameter) pores through the capsid are found at both the I5 and the I3 axes, but these are too small to allow RNA transcript exit without some conformational rearrangement. Regarding such potential rearrangement, capsid elements surrounding each I5 axis of PsV-F appear to be flexible (based on crystallographic temperature factors) (Pan et al., 2009) and so this favors the idea that partitivirus transcripts exit through the I5 pores and that the RdRp is positioned near one of these sites.

One other important aspect of the partitivirus RdRp is that partitivirus transcription is semiconservative (Buck, 1978), meaning that the parental RNA plus strand is released while the progeny RNA plus strand is retained as part of the genomic duplex (i.e., until the next round of transcription when

it is released, etc.). This is also the case for cystovirus transcription, but not for reovirus transcription, which is instead conservative (parental RNA plus strand retained as part of the genomic duplex, progeny RNA plus strand released). Models for reovirus transcription include complex steps for retaining and rewinding the parental plus strand during transcription (Lu et al., 2008; Tao et al., 2002), which are therefore not required as part of partitivirus transcription. Cystovirus transcription is thus likely the better model for partitivirus transcription (Butcher et al., 2001).

With regard to the packaged dsRNA genome structures of PsV-S, PsV-F, and FpV1, there is a bit more to say from the data, but speculation still dominates the interesting considerations. The cryo-TEM structures of all three partitiviruses are marked by concentric rings of RNA densities in the particle interior (Ochoa et al., 2008; Pan et al., 2009; Tang, Ochoa, et al., 2010; Tang, Pan, et al., 2010; Fig. 3.5). These rings have been seen in many other dsRNA viruses and are thought to reflect that the naked (i.e., not protein-coated) dsRNA is packed on average in locally parallel arrays and distributed evenly so as to minimize interhelix spatial and electrostatic conflicts, as first shown for dsDNA bacteriophages (Earnshaw & Harrison, 1977; Maniatis, Venable, & Lerman, 1974). One element of the partitivirus CPs not summarized earlier is that the N-terminal ~40 aa of PsV-S and PsV-F CP are not visualized in the high-resolution structures and thus do not appear in the atomic models (Pan et al., 2009; Tang, Pan, et al., 2010). Notably, though, the first aa visualized in each of these models lies on the undersurface of the capsid (Figs. 3.3C, E and 3.5B), suggesting that the N-terminal peptides plunge into the RNA density regions and thus likely contact the RNA. These RNA contacts may play roles in RNA packaging or synthesis and likely also define where the outermost layer (ring) of RNA is positioned relative to the undersurface of the capsid in the assembled virion. The more-internal RNA layers (rings) may then be subsequently positioned relative to this outer, protein-contacted layer. In the cryo-TEM structures of all three partitiviruses, but especially in PsV-F, these inwardly projecting N termini of the CP subunits (putatively identified as such in FpV1) are also represented by strands or bumps of density that span or enter the space between the capsid undersurface and the outer RNA ring, near the I2 axes (Fig. 3.5).

Given that partitivirus virions become transcriptionally active upon addition of NTPs (Buck, 1978; Pan et al., 2009), there are also interesting structural questions about the genomic and product RNA molecules as they are moved internally to and/or through the capsid shell during transcription.

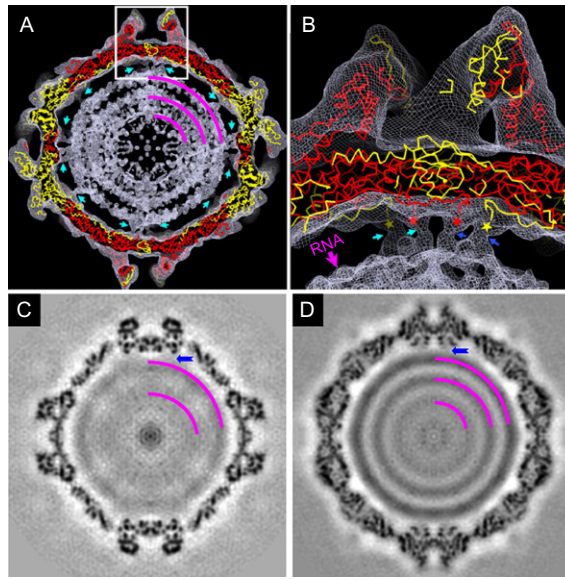

Figure 3.5 Views of genomic dsRNA in fungal partitivirus virions. Equatorial cross sections are shown for PsV-F, PsV-S, and FpV1 cryo-TEM maps. The Cα trace of PsV-F (*A* subunits, red; *B* subunits, yellow) is fitted into the cryo-TEM reconstruction of the PsV-F virion at 8.0-Å resolution. Magenta arcs highlight three rings of RNA density that are evident in the particle interior. Cryo-TEM densities corresponding to the disordered N termini of both subunits (not visible in the Cα traces) are indicated by cyan arrows. A close-up view of the boxed region in (A) is shown in (B). The ordered N-terminal ends of the *A* and *B* subunit Cα traces are indicated by red and yellow stars, respectively. The disordered N-termini from two adjacent *A*–*B* dimers, indicated by cyan and blue arrows, respectively, extend as tube-like densities from the end of the Cα traces into the underlying outer ring of RNA density. (C and D) Density projection images of thin, planar sections encompassing the equatorial regions of (C) PsV-S (Tang, Pan, et al., 2010) and (D) FpV1 (Tang, Ochoa, et al., 2010) are shown. Magenta arcs highlight two or three rings of RNA density evident in PsV-S or FpV1, respectively. Blue arrowheads indicate examples of close approach between the capsid undersurface and the outer RNA ring in both viruses. *(A) and (B) panels have been reproduced from Pan et al. (2009).*

Considering findings with other dsRNA virus RdRps (Butcher et al., 2001; Lu et al., 2008; Tao et al., 2002), our expectation is that the genomic segment of each partitivirus virion is anchored to the internally capsid-bound RdRp in a noncovalent fashion at the end of the dsRNA molecule that includes the 3′ end of the minus-strand RNA, that is, the site of transcription initiation. In this way, the "promoter" region of the minus-strand RNA remains near the RdRp throughout the transcription cycle and therefore

in position to reinitiate transcription at the end of each cycle. In addition, again considering findings with other dsRNA viruses (Diprose et al., 2001; Lawton et al., 1997; Mendez et al., 2008; Yang et al., 2012; Zhang et al., 2003), we expect the partitivirus RdRp is properly positioned so that the parental plus strand, that is, the released product of semiconservative transcription, is directed toward and through a trans-capsid pore for extrusion to the particle exterior for subsequent use in either protein translation or RNA packaging into newly forming virions.

4. COMPARISONS WITH OTHER BISEGMENTED dsRNA VIRUSES

Until recently (see below), there were two other recognized families of dsRNA viruses with bisegmented genomes: *Birnaviridae* and *Picobirnaviridae* (Fig. 3.1). How do birnaviruses and picobirnaviruses compare to the partitiviruses, especially at a structural level? Birnaviruses are known to infect arthropods (insects) and vertebrates (fish, reptiles, and birds; Delmas, Mundt, Vakharia, & Wu, 2011), and picobirnaviruses are known to infect vertebrates (mammals; Delmas, 2011). Thus, their host ranges are quite distinct from those of partitiviruses. One fundamental correlate is that both birnaviruses and picobirnaviruses can undergo regular, extracellular transmission between cells in their complex animal hosts, as well as between host individuals, and thus their virions must contain both the molecular components and the dynamic capabilities for productive cell entry. This is unlike the case for partitiviruses as described earlier. In addition, as a consequence of undergoing extracellular transmission on a regular basis, both birnaviruses and picobirnaviruses are thought to be uniparticulate, that is, to package both of their essential genome segments within each infectious virion, which is again unlike partitiviruses.

Birnaviruses are oddities among encapsidated dsRNA viruses in that they do not contain a 120-subunit capsid. Instead, their single, genome-enclosing capsid is $T=13$, comprising 780 subunits of the main capsid protein VP2 (Coulibaly et al., 2005). This unusual symmetry is the same as that found in the outer capsids of reoviruses and cystoviruses, raising interesting questions with regard to the evolution of these viruses. In any case, the birnavirus capsid is larger and quite distinct from that of partitiviruses.

The story for picobirnaviruses, on the other hand, is quite different. In fact, the CP folds and assembled capsids of rabbit picobirnavirus (RaPBV), the only picobirnavirus for which a 3D structure has been reported to date

(Duquerroy et al., 2009), are quite similar to those of partitiviruses (Tang, Pan, et al., 2010; Fig. 3.6). Of particular note is that the RaPBV capsid exhibits domain swapping within the shell regions of the quasisymmetric *A*–*B* dimer (Fig. 3.6C), thereby arguing for this dimer to be the assembly protomer and well chosen to represent the IAU, as is also the case for partitiviruses. In addition, the RaPBV CP includes an internally inserted "protruding" domain, comparable to the arch domain of partitiviruses, which contributes additional contacts within, and only within, the quasisymmetric *A*–*B* dimer. In fact, additional domain swapping between the *A* and *B* subunits occurs within the protruding domain of RaPBV (Fig. 3.6C). Although the protruding domain contacts in RaPBV do not produce an arch as in PsV-S and PsV-F, they appear to be more similar to those in FpV1. Lastly, the assembly pathway of picobirnaviruses may be similar to that proposed for partitiviruses in that two quasisymmetric *A*–*B* dimers make extensive contacts across each I2 axis in RaPBV, forming

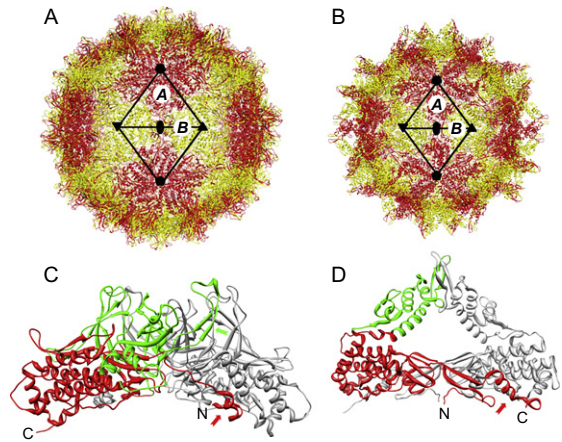

Figure 3.6 Comparison of picobirnavirus and partitivirus capsid organizations and CP folds. Shown are crystallography-derived Cα traces of (A) Rabbit picobirnavirus (RaPBV) virus-like particles (Duquerroy et al., 2009) and (B) partitivirus PsV-F virions (Pan et al., 2009). *A* and *B* subunits are colored red and yellow, respectively. I2, I3, and I5 axes are marked with symbols and connected with lines as in Fig. 3.3. The two capsids are shown at the same scale. Also shown are side views of the Cα traces of the quasisymmetric *A*–*B* dimer of (C) RaPBV and (D) PsV-F. The *B* subunit is colored gray in each. In the *A* subunit, the shell domain is colored red and the protruding/arch domain is colored green. Visible N- and C-termini are labeled for the *A* subunit of each virus. Red arrows point toward an α-helix involved in domain swapping in each virus, as discussed in the text.

compact, diamond-shaped symmetric dimers of dimers (tetramers) in which *A*:*B* contacts between the two dimers occur, but *A*:*A* contacts predominate, again largely through the domain-swapping arms in their shell regions (Fig. 3.6A and C). Thus, the picobirnavirus and partitivirus capsids, as perhaps the viruses themselves, appear to be closely related, probably sharing a unique, common ancestor.

Despite these similarities, it is important to remember that, given their capacity for extracellular transmission, picobirnavirus virions must include the molecular machinery for cell entry (Duquerroy et al., 2009), which partitivirus virions lack. Thus, it seems likely that either the picobirnavirus capsid evolved the capacities for receptor binding and membrane penetration from a common ancestor that lacked them or the partitivirus capsid lost the capacities for receptor binding and membrane penetration from a common ancestor that had them. Regions of the picobirnavirus capsid involved in receptor binding (presumably in the protruding domain) and membrane penetration (presumably hydrophobic and buried in the virion) remain undefined to date. Nonetheless, taking the perspective that partitiviruses likely evolved before picobirnaviruses because their hosts and life styles are simpler, the similar capsid structures of RaPBV and partitiviruses suggest that the path for a nonenveloped virus to acquire cell-entry functions including receptor binding and membrane penetration may be relatively uncomplicated, without a need for major architectural changes to the capsid. Note that partitivirus virions can in fact initiate *de novo* infection of fungal protoplasts when transfection methods that bypass the need for virion-inherent entry machinery are used (Kanematsu, Sasaki, Onoue, Oikawa, & Ito, 2010; Sasaki, Kanematsu, Onoue, Oyama, & Yoshida, 2006). Thus, the partitivirus virion appears to be a potentially infectious "payload" that simply lacks the necessary, built-in components for efficient payload delivery from outside cells.

Two other general properties of picobirnaviruses suggest several interesting questions upon comparison with partitiviruses. One is the presumed packaging of both of the two essential genome segments of picobirnaviruses into the same infectious particle, which is not the case for partitiviruses. What changes in the picobirnavirus or partitivirus CP might have been needed to evolve in order to accommodate this difference in packaging strategy? Are there two copies of packaged RdRp, one for each segment, in the picobirnavirus virion? Is there indeed enough room in the central cavity of the picobirnavirus virion to hold both segments in addition to probably two copies of RdRp? The other property in question is the style of transcription

by picobirnavirus virions. Is it semiconservative as with partitiviruses, or is it instead conservative as with many other encapsidated dsRNA viruses? Because infectious, genome-containing picobirnavirus virions have been difficult to isolate in sufficient quantities to date (note that the RaPBV crystal structure is that of virus-like particles assembled after CP expression in insect cells), this relatively simple question remains unanswered.

A fourth family of bisegmented dsRNA viruses, *Megabirnaviridae*, has been recently recognized (Fig. 3.1). To date, it is represented by a single characterized strain, Rosellinia necatrix megabirnavirus 1, from the phytopathogenic ascomycete *Rosellinia necatrix*, which is the cause of white root rot in fruit trees worldwide (Chiba et al., 2009). The 3D structure of this virus has yet to be reported, but the virions appear to be somewhat larger than those of partitiviruses, ~50 nm in diameter. The genome is also larger, comprising 8931-bp dsRNA1 and 7180-bp dsRNA2, with both the CP and the RdRp encoded on dsRNA1. More detailed comparisons with partitiviruses await further characterizations.

5. COMPARISONS WITH OTHER FUNGAL VIRUSES WITH ENCAPSIDATED dsRNA GENOMES

Other fungal viruses with encapsidated dsRNA genomes are currently found in four other families: *Totiviridae* (one genome segment, >4.5 kbp), *Chrysoviridae* (four segments, >11 kbp in total), *Quadriviridae* (four segments, >16 kbp in total), and *Reoviridae* (9–12 segments, >18 kbp in total; 11 or 12 segments in members of the genus *Mycoreovirus*; Fig. 3.1). Representative structures are available for three of these families (all but *Quadriviridae*; Lin et al., 2012), and indeed 3D structures of fungal virus strains are available for both totiviruses and chrysoviruses (Castón et al., 2006; Cheng et al., 1994; Gómez-Blanco et al., 2012; Luque et al., 2010; Naitow et al., 2002). All have genome-enclosing capsids or inner capsids with $T=1$ icosahedral symmetry, like partitiviruses, but despite this basic similarity, there are a number of differences.

Totivirus capsids and reovirus inner capsids are 120-subunit $T=1$ structures, like those of partitiviruses, but their subunit architectures are relatively thinner in the radial direction. Their respective CPs and ICPs are thus often described as "plate-like" and generally lack the sort of major protruding regions as possessed by partitivirus (and RaPBV) CPs. In addition, the totivirus CPs and reovirus ICPs are commonly described as having two or three different domains within their shell regions and are therefore more elongated

(Dunn et al., 2013; Grimes et al., 1998; McClain et al., 2010; Naitow et al., 2002; Reinisch et al., 2000; Tang et al., 2008; Yu et al., 2008; Zhou et al., 2001; see Fig. 3.4A), whereas partitiviruses are described as having a single shell domain, with a second domain protruding above the shell (Pan et al., 2009; Tang, Pan, et al., 2010; see Fig. 3.3C and E). Although totivirus CPs are generally somewhat larger in molecular mass (>70 kDa), reovirus ICPs are consistently even larger (>100 kDa). As a consequence of these different protein structures and sizes, the central cavity enclosed by totivirus capsids and reovirus inner capsids is a good deal larger than that enclosed by partitivirus capsids, consistent with the different amounts of dsRNA being packaged inside each. Other differences in describing the IAUs and potential assembly pathways of these viruses are discussed earlier.

The capsid of chrysoviruses is even more distinct (Gómez-Blanco et al., 2012; Luque et al., 2010). Though also exhibiting $T=1$ icosahedral symmetry, it is a "simple" $T=1$ formed from only 60 CP subunits per virion. The chrysovirus CP is relatively large, however, more similar in molecular mass (>100 kDa) to the ICPs of reoviruses, and has been shown to reflect a genetic duplication, such that each monomeric CP subunit contains two structurally similar shell domains. As a result, the chrysovirus capsid is in fact structurally similar to that of the 120-subunit dsRNA viruses, including partitiviruses. Since an atomic model of the chrysovirus CP is not available to date, it is not yet known with certainty whether the two shell domains in each monomer reside side by side or end to end within the capsid, adopting respectively either a more or a less compact form that would likely impact the pathway of chrysovirus capsid assembly.

An additional point of importance for comparison is that the genome-enclosing CPs or ICPs of totiviruses, partitiviruses, picobirnaviruses, cystoviruses, chrysoviruses, and reoviruses, all of which form $T=1$ structures, are also all relatively rich in α-helices within their shell domains (see Fig. 3.6, top). Furthermore, it appears from comparisons of these structures that certain key α-helices may be widely conserved in their approximate structural placements and interactions within many of these proteins (Dunn et al., 2013; Luque et al., 2010; Ochoa et al., 2008). This suggests that an ancient, ancestral helix-rich CP with the capacity for $T=1$ capsid assembly might be common to many or all of the encapsidated dsRNA viruses that have been studied to date, with the exception of birnaviruses. The main capsid protein of birnaviruses, in contrast, which forms a $T=13$ structure, is richer in β-sheets and related to the β-rich jelly-roll structures of many plus-strand RNA virus capsid subunits (Coulibaly et al., 2005).

6. PROPOSED REVISIONS TO PARTITIVIRUS TAXONOMY

Earlier in this review, we suggested that the family *Partitiviridae* is due for some taxonomic revisions, based on a recent accumulation of genomic sequence data and phylogenetic analyses that have called some of the previous taxonomic groupings into question (Boccardo & Candresse, 2005; Crawford et al., 2006; Ghabrial et al., 2008, 2011; Tang, Ochoa, et al., 2010; Willenborg et al., 2009). One such suggested revision, discussed earlier, is to divide the genus *Partitivirus* into two new genera (Fig. 3.7). Regarding the viruses whose structures we have determined, PsV-S and PsV-F would be placed in one of these new genera, whereas FpV1 would be placed in the other, along with the *Partitivirus* prototype strain AhV. It is helpful to note that the 3D structures of these viruses, emphasized in this review, concur with this division, in that the PsV-S and PsV-F capsids are more similar to one another than either is to the FpV1 capsid (Ochoa et al., 2008; Pan et al., 2009; Tang, Ochoa, et al., 2010, Tang, Pan, et al., 2010).

One interesting side note here is that the putative new genus containing FpV1 and AhV, based on phylogenetic results, would also contain at least two viruses that seem to have been isolated from plants, *Primula malacoides* and *Cannabis sativa* (Li, Tian, Du, Duns, & Chen, 2009; Ziegler, Matoušek, Steger, & Schubert, 2012; Fig. 3.7). Previously, host range has been considered an important determinant for drawing genus divisions, and thus fungal partitiviruses have been placed in the genus *Partitivirus* while plant partitiviruses have been placed in the genus *Alphacryptovirus* or the genus *Betacryptovirus* depending on certain phenotypic characteristics. Sequence-based phylogenetic results, however, including the ones described earlier, suggest that fungal versus plant host range may not be a proper criterion for drawing genus divisions for at least some partitiviruses. There remains the possibility that the partitiviruses of *P. malacoides* and *C. sativa* were in fact derived from contaminating fungi, perhaps pathogens or symbionts of these plants, but the other possible interpretation is that partitiviruses can transfer across the fungus–plant host boundary over evolutionary time periods, perhaps through cross-feeding insects or other vectors, or perhaps simply through the intimate association of certain fungi with their plant hosts. Indeed, recent evidence for integration into plant genomes by partitivirus sequences related to ones from fungi, suggesting horizontal gene transfer, also supports the notion of a common ancestor of fungal and plant partitiviruses, consistent with their possible inclusion in the same, modern genus (Chiba et al., 2011; Liu et al., 2011).

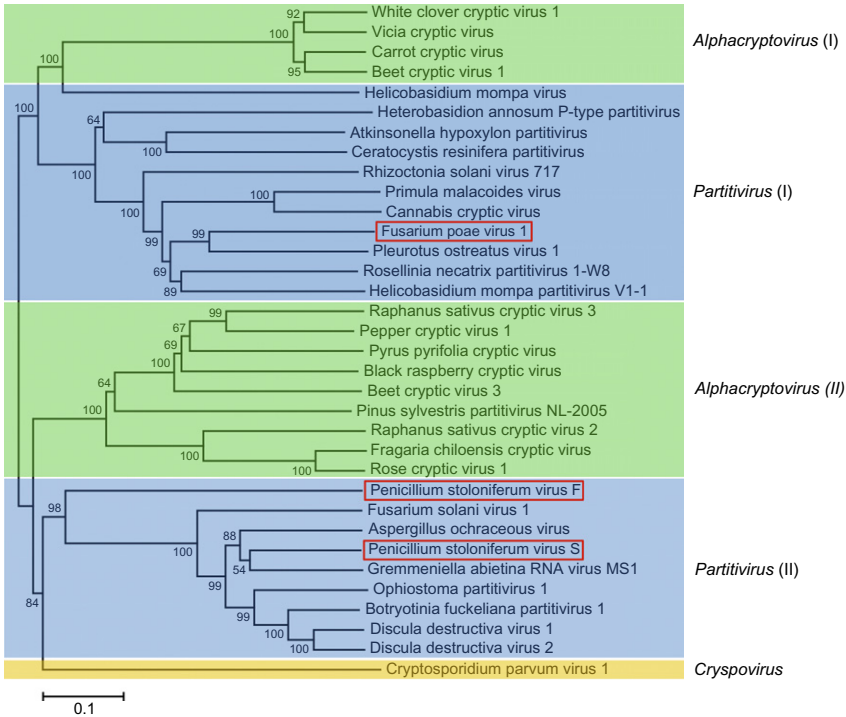

Figure 3.7 Neighbor-joining phylogenetic tree for the family *Partitiviridae*. The tree was constructed from complete aa sequences of RdRps of representative members and probable members of the family. The aa sequences were aligned using the program CLUSTAL X2, and the tree was generated for codon positions using the MEGA5 phylogenetic package. Bootstrap percentages out of 2000 replicates are indicated at the nodes. Green, blue, and yellow shading, respectively, highlight the assignments of individual viruses to the current genera *Alphacryptovirus*, *Partitivirus*, and *Cryspovirus*. The divisions of the *Alphacryptovirus* and *Partitivirus* regions into two sections each (I, II) reflect the four new genera, obtained by dividing the current genera, that are suggested by these and previous phylogenetic results as cited in the text. Red boxes indicate the three fungal partitiviruses for which 3D structures are described in recent reports and this review. GenBank accession numbers for the viruses in this figure are, top to bottom: YP_086754, ABN71237, ACL93278, YP_002308574, BAC23065, AF473549, NP_604475, YP_001936016, NP_620659, YP_00310476, AET80948, NP_624349, YP_227355, YP_392480, BAD32677, ACJ76981, ABC96789, BAA34783, ABU55400, AAB27624, AAY51483, ABB04855, AAZ06131, ABZ10945, YP_271922, BAA09520, ABV30675, AAN8683, NP_659027, CAJ31886, YP_001686789, AAG59816, NP_620301, and AAC47805.

Another suggested revision based on phylogenetic results is to divide the genus *Alphacryptovirus* into two new genera as well (Boccardo & Candresse, 2005; Crawford et al., 2006; Ghabrial et al., 2008, 2011; Willenborg et al., 2009). In this case, it is again notable that one of the putative new genera, that including the *Alphacryptovirus* prototype white clover cryptic virus (Fig. 3.7), includes both plant isolates and at least one fungal isolate (Helicobasidium mompa virus in Fig. 3.7). Thus, the considerations noted above again pertain, suggesting that fungal versus plant host range may not be a proper criterion for drawing genus divisions for some partitiviruses. The status of the genus *Betacryptovirus* in the revised taxonomy remains unclear because no sequences from members of that genus have been reported to date. The genus *Cryspovirus*, containing isolates from the apicomplexan protozoan *Cryptosporidium*, on the other hand, appears to remain on solid footing as a divergent taxon within this family (Nibert et al., 2009; Fig. 3.7). In moving ahead to propose these taxonomic changes in a formal manner to the International Committee on Taxonomy of Viruses, additional 3D structures, from members of the other current and proposed genera, would be helpful.

The highly similar CP and capsid structures of RaPBV and partitiviruses contribute to raising another taxonomic question, namely, whether picobirnaviruses and partitiviruses should indeed have been separated into two families. Given several other fundamental properties that differ between these virus groups as described earlier, we consider their current separation into two families to remain quite appropriate. Nevertheless, addition of a superfamily designation to encompass both families *Picobirnaviridae* and *Partitiviridae*, for example, reflecting their putatively more recent common ancestor, might be something to consider.

ACKNOWLEDGMENTS

This work was supported in part by NIH grants R37-GM033050 and 1S10-RR020016 (T. S. B.), by Kentucky Science and Engineering Foundation grant KSEF-2178-RDE-013 (S. A. G.), and by Welch Foundation grant C-1565 (Y. J. T.). The San Diego Supercomputer Center provided access to TeraGrid computing, and support from the University of California–San Diego and the Agouron Foundation (T. S. B.) were used to establish and equip cryo-TEM facilities at the University of California–San Diego.

REFERENCES

Boccardo, G., & Candresse, T. (2005). Complete sequence of the RNA1 of an isolate of *White clover cryptic virus 1*, type species of the genus *Alphacryptovirus*. *Archives of Virology*, *150*, 399–402.

Bozarth, R. F., Wood, H. A., & Mandelbrot, A. (1971). The Penicillium stoloniferum virus complex: Two similar double-stranded RNA virus-like particles in a single cell. *Virology*, *45*, 516–523.

Bruenn, J. A. (1993). A closely related group of RNA-dependent RNA polymerases from double-stranded RNA viruses. *Nucleic Acids Research*, *21*, 5667–5669.

Buck, K. W. (1978). Semi-conservative replication of double-stranded RNA by a virion-associated RNA polymerase. *Biochemical and Biophysical Research Communications*, *84*, 639–645.

Buck, K. W., & Kempson-Jones, G. F. (1973). Biophysical properties of Penicillium stoloniferum virus S. *Journal of General Virology*, *18*, 223–235.

Buck, K. W., & Kempson-Jones, G. F. (1974). Capsid polypeptides of two viruses isolated from *Penicillium stoloniferum*. *Journal of General Virology*, *22*, 441–445.

Butcher, S. J., Grimes, J. M., Makeyev, E. V., Bamford, D. H., & Stuart, D. I. (2001). A mechanism for initiating RNA-dependent RNA polymerization. *Nature*, *410*, 235–240.

Castón, R. J., Luque, D., Trus, B. L., Rivas, G., Alfonso, C., González, J. M., et al. (2006). Three-dimensional structure and stoichiometry of Helminthosporium victoriae 190S totivirus. *Virology*, *347*, 323–332.

Castón, J. R., Trus, B. L., Booy, F. P., Wickner, R. B., Wall, J. S., & Steven, A. C. (1997). Structure of L-A virus: A specialized compartment for the transcription and replication of double-stranded RNA. *The Journal of Cell Biology*, *138*, 975–985.

Cheng, R. H., Caston, J. R., Wang, G.-J., Gu, F., Smith, T. J., Baker, T. S., et al. (1994). Fungal virus capsids, cytoplasmic compartments for the replication of double-stranded RNA, formed as icosahedral shells of asymmetric gag dimers. *Journal of Molecular Biology*, *244*, 255–258.

Chiba, S., Kondo, H., Tani, A., Saisho, D., Sakamoto, W., Kanematsu, S., et al. (2011). Widespread endogenization of genome sequences of non-retroviral RNA viruses into plant genomes. *PLoS Pathogens*, *7*, e1002146.

Chiba, S., Salaipeth, L., Lin, Y. H., Sasaki, A., Kanematsu, S., & Suzuki, N. (2009). A novel bipartite double-stranded RNA mycovirus from the white root rot fungus *Rosellinia necatrix*: Molecular and biological characterization, taxonomic considerations, and potential for biological control. *Journal of Virology*, *83*, 12801–12812.

Compel, P., Papp, I., Bibo, M., Fekete, C., & Hornok, L. (1999). Genetic relationships and genome organization of double-stranded RNA elements of *Fusarium poae*. *Virus Genes*, *18*, 49–56.

Coulibaly, F., Chevalier, C., Gutsche, I., Pous, J., Navaza, J., Bressanelli, S., et al. (2005). The birnavirus crystal structure reveals structural relationships among icosahedral viruses. *Cell*, *120*, 761–772.

Crawford, L. J., Osman, T. A., Booy, F. P., Coutts, R. H., Brasier, C. M., & Buck, K. W. (2006). Molecular characterization of a partitivirus from *Ophiostoma himal-ulmi*. *Virus Genes*, *33*, 33–39.

Delmas, B. (2011). Picobirnaviridae. In A. M. Q. King, M. J. Adams, E. B. Carstens & E. J. Lefkowitz (Eds.), *Virus taxonomy: Ninth report of the international committee on taxonomy of viruses* (pp. 535–539). Oxford, UK: Elsevier.

Delmas, B., Mundt, E., Vakharia, V. N., & Wu, J. L. (2011). Birnaviridae. In A. M. Q. King, M. J. Adams, E. B. Carstens & E. J. Lefkowitz (Eds.), *Virus taxonomy: Ninth report of the international committee on taxonomy of viruses* (pp. 499–507). Oxford, UK: Elsevier.

Diprose, J. M., Burroughs, J. N., Sutton, G. C., Goldsmith, A., Gouet, P., Malby, R., et al. (2001). Translocation portals for the substrates and products of a viral transcription complex: The bluetongue virus core. *The EMBO Journal*, *20*, 7229–7239.

Dunn, S. E., Li, H., Cardone, G., Nibert, M. L., Ghabrial, S. A., and Baker, T. S. (2013). Three-dimensional structure of the genus *Victorivirus* prototype strain HvV190S suggests

that the capsid proteins in all totiviruses may share a conserved core. PLOS Pathogens, in press.

Duquerroy, S., Da Costa, B., Henry, C., Vigouroux, A., Libersou, S., Lepault, J., et al. (2009). The picobirnavirus crystal structure provides functional insights into virion assembly and cell entry. *The EMBO Journal*, *28*, 1655–1665.

Earnshaw, W. C., & Harrison, S. C. (1977). DNA arrangement in isometric phage heads. *Nature*, *268*, 598–602.

Ghabrial, S. A., Nibert, M. L., Maiss, E., Lesker, T., Baker, T. S., & Tao, Y. J. (2011). Partitiviridae. In A. M. Q. King, M. J. Adams, E. B. Carstens & E. J. Lefkowitz (Eds.), *Virus taxonomy: Ninth report of the international committee on taxonomy of viruses* (pp. 523–534). Oxford, UK: Elsevier.

Ghabrial, S. A., Ochoa, W. F., Baker, T. S., & Nibert, M. L. (2008). Partitiviruses: General features. In B. W. J. Mahy & M. H. V. van Regenmortel (Eds.), (3rd ed.). *Encyclopedia of virology*, Vol. 4, (pp. 68–75). Oxford, UK: Elsevier.

Gómez-Blanco, J., Luque, D., González, J. M., Carrascosa, J. L., Alfonso, C., Trus, B., et al. (2012). Cryphonectria nitschkei virus 1 structure shows that the capsid protein of chrysoviruses is a duplicated helix-rich fold conserved in fungal double-stranded RNA viruses. *Journal of Virology*, *86*, 8314–8318.

Grimes, J. M., Burroughs, J. N., Gouet, P., Diprose, J. M., Malby, R., Ziéntara, S., et al. (1998). The atomic structure of the bluetongue virus core. *Nature*, *395*, 470–478.

Huiskonen, J. T., de Haas, F., Bubeck, D., Bamford, D. H., Fuller, S. D., & Butcher, S. J. (2006). Structure of the bacteriophage ϕ6 nucleocapsid suggests a mechanism for sequential RNA packaging. *Structure*, *14*, 1039–1048.

Kainov, D. E., Butcher, S. J., Bamford, D. H., & Tuma, R. (2003). Conserved intermediates on the assembly pathway of double-stranded RNA bacteriophages. *Journal of Molecular Biology*, *328*, 791–804.

Kanematsu, S., Sasaki, A., Onoue, M., Oikawa, Y., & Ito, T. (2010). Extending the fungal host range of a partitivirus and a mycoreovirus from *Rosellinia necatrix* by inoculation of protoplasts with virus particles. *Phytopathology*, *100*, 922–930.

Kim, J. W., Choi, E. Y., & Lee, J. I. (2005). Genome organization and expression of the Penicillium stoloniferum virus F. *Virus Genes*, *31*, 175–183.

Kim, J. W., Kim, S. Y., & Kim, K. M. (2003). Genome organization and expression of the Penicillium stoloniferum virus S. *Virus Genes*, *27*, 249–256.

Lawton, J. A., Estes, M. K., & Prasad, B. V. V. (1997). Three-dimensional visualization of mRNA release from actively transcribing rotavirus particles. *Nature Structural Biology*, *4*, 118–121.

Li, L., Tian, Q., Du, Z., Duns, G. J., & Chen, J. (2009). A novel double-stranded RNA virus detected in *Primula malacoides* is a plant-isolated partitivirus closely related to partitivirus infecting fungal species. *Archives of Virology*, *154*, 565–572.

Lin, Y. H., Chiba, S., Tani, A., Kondo, H., Sasaki, A., Kanematsu, S., et al. (2012). A novel quadripartite dsRNA virus isolated from a phytopathogenic filamentous fungus, *Rosellinia necatrix*. *Virology*, *426*, 42–50.

Liu, H., Fu, Y., Xie, J., Cheng, J., Ghabrial, S. A., Li, G., et al. (2011). Widespread horizontal gene transfer from double-stranded RNA viruses to eukaryotic nuclear genomes. *Journal of Virology*, *84*, 11876–11887.

Lu, X., McDonald, S. M., Tortorici, M. A., Tao, Y. J., Vasquez-Del Carpio, R., Nibert, M. L., et al. (2008). Mechanism for coordinated RNA packaging and genome replication by rotavirus polymerase VP1. *Structure*, *16*, 1678–1688.

Luque, D., González, J. M., Garriga, D., Ghabrial, S. A., Havens, W. M., Trus, B., et al. (2010). The T=1 capsid protein of Penicillium chrysogenum virus is formed by a repeated helix-rich core indicative of gene duplication. *Journal of Virology*, *84*, 7256–7266.

Maniatis, T., Venable, J. H., Jr., & Lerman, L. S. (1974). The structure of psi DNA. *Journal of Molecular Biology*, *84*, 37–64.

McClain, B., Settembre, E., Temple, B. R., Bellamy, A. R., & Harrison, S. C. (2010). X-ray crystal structure of the rotavirus inner capsid particle at 3.8 Å resolution. *Journal of Molecular Biology*, *397*, 587–599.

Mendez, I. I., Weiner, S. G., She, Y. M., Yeager, M., & Coombs, K. M. (2008). Conformational changes accompany activation of reovirus RNA-dependent RNA transcription. *Journal of Structural Biology*, *162*, 277–289.

Naitow, H., Tang, J., Canady, M., Wickner, R. B., & Johnson, J. E. (2002). L-A virus at 3.4 Å resolution reveals particle architecture and mRNA decapping mechanism. *Nature Structural Biology*, *9*, 725–728.

Nibert, M. L., Woods, K. M., Upton, S. J., & Ghabrial, S. A. (2009). *Cryspovirus*: A new genus of protozoan viruses in the family *Partitiviridae*. *Archives of Virology*, *154*, 1959–1965.

Ochoa, W. F., Havens, W. M., Sinkovits, R. S., Nibert, M. L., Ghabrial, S. A., & Baker, T. S. (2008). Partitivirus structure reveals a 120-subunit, helix-rich capsid with distinctive surface arches formed by quasisymmetric coat-protein dimers. *Structure*, *16*, 776–786.

Oh, C. S., & Hillman, B. I. (1995). Genome organization of a partitivirus from the filamentous ascomycete *Atkinsonella hypoxylon*. *Journal of General Virology*, *76*, 1461–1470.

Ortín, J., & Parra, F. (2006). Structure and function of RNA replication. *Annual Review of Microbiology*, *60*, 305–326.

Pan, J., Dong, L., Lin, L., Ochoa, W. F., Sinkovits, R. S., Havens, W. M., et al. (2009). Atomic structure reveals the unique capsid organization of a dsRNA virus. *Proceedings of the National Academy of Sciences of the United States of America*, *106*, 4225–4230.

Pan, J., Vakharia, V. N., & Tao, Y. J. (2007). The structure of a birnavirus polymerase reveals a distinct active site topology. *Proceedings of the National Academy of Sciences of the United States of America*, *104*, 7385–7390.

Reinisch, K. M., Nibert, M. L., & Harrison, S. C. (2000). Structure of the reovirus core at 3.6-Å resolution. *Nature*, *404*, 960–967.

Sasaki, A., Kanematsu, S., Onoue, M., Oyama, Y., & Yoshida, K. (2006). Infection of *Rosellinia necatrix* with purified viral particles of a member of *Partitiviridae* (RnPV1-W8). *Archives of Virology*, *151*, 697–707.

Sen, A., Heymann, J. B., Cheng, N., Qiao, J., Mindich, L., & Steven, A. C. (2008). Initial location of the RNA-dependent RNA polymerase in the bacteriophage ϕ6 procapsid determined by cryo-electron microscopy. *The Journal of Biological Chemistry*, *283*, 12227–12231.

Tang, J., Ochoa, W. F., Li, H., Havens, W. M., Nibert, M. L., Ghabrial, S. A., et al. (2010). Structure of Fusarium poae virus 1 shows conserved and variable elements of partitivirus capsids and evolutionary relationships to picobirnavirus. *Journal of Structural Biology*, *172*, 363–371.

Tang, J., Ochoa, W. F., Sinkovits, R. S., Poulos, B. T., Ghabrial, S. A., Lightner, D. V., et al. (2008). Infectious myonecrosis virus has a totivirus-like, 120-subunit capsid, but with fiber complexes at the fivefold axes. *Proceedings of the National Academy of Sciences of the United States of America*, *105*, 17526–17531.

Tang, J., Pan, J., Havens, W. M., Ochoa, W. F., Guu, T. S., Ghabrial, S. A., et al. (2010). Backbone trace of partitivirus capsid protein from electron cryomicroscopy and homology modeling. *Biophysical Journal*, *99*, 685–694.

Tao, Y., Farsetta, D. L., Nibert, M. L., & Harrison, S. C. (2002). RNA synthesis in a cage—Structural studies of reovirus polymerase λ3. *Cell*, *111*, 733–745.

Willenborg, J., Menzel, W., Vetten, H. J., & Maiss, E. (2009). Molecular characterization of two alphacryptovirus dsRNAs isolated from *Daucus carota*. *Archives of Virology*, *154*, 541–543.

Yang, C., Ji, G., Liu, H., Zhang, K., Liu, G., Sun, F., et al. (2012). Cryo-EM structure of a transcribing cypovirus. *Proceedings of the National Academy of Sciences of the United States of America*, *109*, 6118–6123.

Yu, X., Jin, L., & Zhou, Z. H. (2008). 3.88 Å structure of cytoplasmic polyhedrosis virus by cryo-electron microscopy. *Nature*, *453*, 415–419.

Zhang, X., Walker, S. B., Chipman, P. R., Nibert, M. L., & Baker, T. S. (2003). Reovirus polymerase λ3 localized by cryo-electron microscopy of virions at a resolution of 7.6 Å. *Nature Structural Biology*, *10*, 1011–1018.

Zhou, Z. H., Baker, M. L., Jiang, W., Dougherty, M., Jakana, J., Dong, G., et al. (2001). Electron cryomicroscopy and bioinformatics suggest protein fold models for rice dwarf virus. *Nature Structural Biology*, *8*, 868–873.

Ziegler, A., Matoušek, J., Steger, G., & Schubert, J. (2012). Complete sequence of a cryptic virus from hemp (*Cannabis sativa*). *Archives of Virology*, *157*, 383–385.